

Numerical modelling of fin side heat transfer and pressure loss for compact heat recovery steam generators

Johan R. Espelund ^{a,b*}, Ole H. H. Meyer ^b, Geir Skaugen ^b

^a NTNU - Department of Energy and Process Engineering, ^b SINTEF Energy Research,
johan.espelund@sintef.no

Abstract

An optimization tool for offshore bottoming cycle and heat recovery steam generator (HRSG) design has previously been developed. The tool is based on empirical correlations to obtain hydraulic and thermal quantities for the HRSG. However, as these correlations are based on experiments with typical onshore designs, they may not be valid for the compact designs encountered in offshore HRSGs.

In order to extend the validity range of the optimization tool, this work presents a numerical model able to predict heat transfer and pressure loss in finned tube bundles by means of Computational Fluid Dynamics (CFD), utilizing a periodic domain to reduce computational costs. Both steady-state and transient models were applied, using the Spalart-Allmaras turbulence model, and their performance compared. To validate the model, results were compared with available experimental data, and then the model's performance was compared with a selected empirical correlation.

Three different fin-tube geometries were investigated (two serrated and solid) with varying tube layout angles. A parameterized grid generation tool was developed and used to generate grids for the selected geometries. The CFD results were found to be within 20 % of the experimental data, and were in most cases more accurate than the empirical correlation. The steady-state simulations did, however, not converge for the geometry with the largest layout angle. The steady-state framework should therefore be applied only to compact tube layouts. The transient simulations, though being computationally more intensive, are also able to model large layout angles.

1. Introduction

Oil and gas production contributes significantly to the global CO₂-emissions. In Norway, it is the industry that emits most greenhouse gases, accounting for 27% of CO₂-emissions from Norwegian territory in 2019. The largest contributor to these emissions are the gas turbines used for power generation offshore, which amounts to around 85% of these emissions. [1]

The large emissions of the gas turbines makes them an attractive candidate for emission reduction, and installing steam bottoming cycles has been proposed as a way to achieve this. Most of today's offshore power systems utilize the hot exhaust gases to some degree, e.g. for heating crude oil, but the heat lost to the atmosphere is still significant. With a steam bottoming cycle the heat is utilized for power generation using a steam generator, lowering the demand for power production from the gas turbines, and can reduce the turbine CO₂-emissions with as much as 25% [2]. One reason for why there is no widespread use of offshore steam bottoming cycles today, is weight and size limitations.

The heat recovery steam generator (HRSG) is a crucial and large component of the steam bottoming cycle. The limitations necessitate compact designs, and the once through steam generator (OTSG) has been found to be the most suitable HRSG type for offshore steam bottoming cycles [2]. One of the key factors when optimizing OTSGs for weight and size is small diameter heat exchanger tubes, compared with their onshore equivalents [3, 4].

The optimization procedures used in the design process rely on correlations for finned tube banks in order to

predict the heat transfer and pressure drop of the OTSG. Correlations are almost exclusively based on empirical data, and their region of validity is therefore limited to the range of experiments that they are based on. This has proved to be a challenge for the optimization of the compact offshore OTSG designs, which have fin and tube geometries outside the validity range of the correlations. The result is that different correlations tend to give significantly different predictions when compared to the same experimental data sets. Holfeld [5] reported up to 77% spread between the correlations for heat transfer, and up to 410% for pressure drop when comparing different correlations to the same experimental data.

Ideally, new correlations would be developed based on experiments that are performed under conditions close to those expected for the offshore OTSGs. However, performing experiments to produce enough data for new correlation development is both costly and time-consuming, and therefore Computational Fluid Dynamics (CFD) is proposed as a way to predict heat transfer and pressure drop in compact OTSGs, and to validate the designs produced by the optimization procedure.

Numerical simulations of finned tube banks, and particularly serrated fins, have only started to emerge in the course of the last two decades, as CFD has become more widespread in the engineering field and the computational power available to researchers and engineers has increased. The earliest works on the field were limited to solid annular fins, with few tube rows being modelled. Jang et al. [6] performed both experiments and numerical modelling of

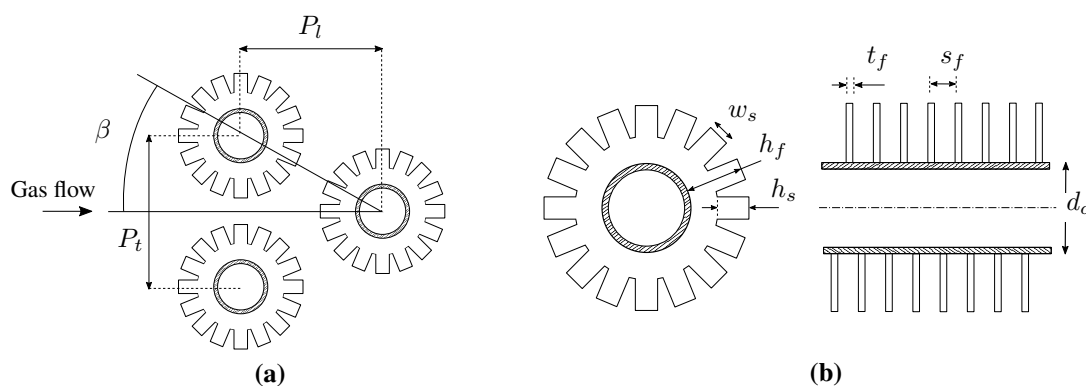


Figure 1: (a) Tube layout parameters. (b) Fin and tube geometry parameters

laminar flow through 4 tube rows in a staggered layout. The numerical model was able to accurately predict pressure drop, but over-estimated heat transfer by 20 - 30%.

Mon [7] performed turbulent simulations for 23 different tube layouts, both in-line and staggered, with the number of tube rows ranging from 2 to 6. The model was able to qualitatively describe the flow, but no comparison with experimental data was done. New correlations based on the numerical results and available experimental data were proposed. In a later paper, Mon & Gross [8] compared the results from selected layouts with existing correlations, where they were found to agree from $\pm 15\%$ to over 50%. Torresi et al. [9] were among the first to model flow in tube banks with serrated fins. They simulated only one tube row, without modelling heat transfer, and then used equivalent porous medium zones in order to model the full HRSG. The results were not compared with experimental data, but showed good agreement with a proprietary 1D code.

McIlwian [10] compared the performance of solid and serrated fins in a single tube row, and gave qualitative insight into how serrated fins improve heat transfer compared with solid fins. In a later study [11], McIlwian extended the model and looked at the effects of adding a 2nd, 3rd and 4th row. The results were compared with correlations, but neither of the studies were validated with experimental data.

As with Jang et al., laminar flow was also assumed by Lemouedda et al. [12], where fin tube bundles for Re between 600 and 2 600 were investigated. Fins with and without serration were compared, and the effect of twisting of the serrated fins was also investigated. No comparisons with experiments were made.

Hofmann & Walter [13] performed simulations and experiments for both solid and serrated fins, with both helical and angular fin attachment. Both local and overall heat transfer and pressure drop was investigated for turbulent flow with Re ranging from 3500 to 50 000. Results showed good agreement of the simulations with experimental data, being within $\pm 15\%$ uncertainty.

Ó Cléirigh and Smith [14] investigated the effects of degree of serration, modelling fully serrated, partially serrated and solid fins. They found that the Nusselt number increased with 23% from partially to fully serrated fins, a distinction that is not made in most correlations. However, no validation against experimental data was performed in this study either.

Where the previous studies all have used standard inlet-outlet boundary conditions in the stream wise direction, Martinez et al. [15] utilized periodic boundary conditions also in this direction, thus assuming fully periodic flow. Local flow features were compared with experimental

measurements, but global heat transfer and pressure drop were only compared with selected correlations, though with good agreement. In a consecutive paper [16], they went on to model six tube rows using standard inlet-outlet boundary condition, and showed that the velocity, temperature and turbulence fields indeed display periodic behaviour after the third tube row.

Lindqvist & Næss [17] also used a periodic domain model, and applied it to four different cases, both serrated and solid fins. For one of them, a full domain model with eight tube rows was also considered, which was shown to match very closely with the periodic domain model. All four cases were validated against experimental data, and were found to be within 15% for both heat transfer and pressure drop. In addition, three correlations and two fin efficiency corrections were compared with the numerical and experimental results and their performances assessed. In a consecutive study [18], the authors investigated vortex-shedding frequencies by performing transient simulations with the same model, not including heat transfer. Both studies were limited to geometries with compact tube layout angles of 30° .

The aim of the present work is to develop a numerical model that is able to readily and accurately predict heat transfer and pressure drop for a range of geometrical parameters that is representative of compact heat exchangers. Both serrated and solid fins will be considered, and will be restricted to helical fin attachment. Both steady-state and transient simulations will be carried out and their performance assessed. To model a wider range of fin-tube geometries, the present work will use geometries with different layout-angles. The model will be validated with available experimental data and compared with an empirical correlation.

2. Selected geometries

Solid and serrated fin tubes are characterized by a fixed set of parameters, illustrated in Fig. 1b, with the solid fin being a special case of the serrated fin ($h_s = 0$). The tube bundle layout is characterized by the longitudinal and transverse pitches P_l and P_t , respectively, or the tube layout angle $\beta = \arctan\left(\frac{P_t}{2P_l}\right)$, as shown in Fig. 1a.

The three tube and fin geometries considered in this study, listed in Tab. 1, are selected in order to span a sufficiently wide range of parameters to represent the possible designs encountered in compact heat exchangers. The first two geometries, N1 and N2, are geometries 1 and 2 from the experimental study by Næss [19], respectively. The two cases from Næss are using the same serrated fin tube geometry, but with different layout angles. Næss showed that correlations tended to perform poorly for serrated

Table 1: Layout, fin and tube geometries that are modelled.

Geometry Type	H8	N1	N2
P_t [mm]	38.7	46.1	65.2
P_l [mm]	33.5	39.9	32.6
d_o [mm]	13.5	20.89	20.89
h_f [mm]	10	8.61	8.61
h_s [mm]	-	8.61	8.61
s_f [mm]	2.81	5.08	5.08
t_f [mm]	0.50	0.91	0.91
w_f [mm]	-	3.97	3.97
β [°]	30	30	45

geometries with layout angles deviating from 30°, and it is therefore desirable to investigate the predictive accuracy of the numerical model in this case. The third case, H8, is based on geometry 8 from the experimental study by Holfeld [5], and is a solid finned tube with the same layout angle as N1 (30°).

3. Numerical method

The open-source CFD library OpenFOAM v2112 was used to solve the coupled equations and SALOME v6.7.0 was used for the grid generation.

3.1. Domain

The numerical domain consists of two regions: a fluid region (gas) and a solid region (fins), as conduction in the fins is also modelled. Note that only the outer surface of the tube is modelled, *not* the tube wall itself. The numerical

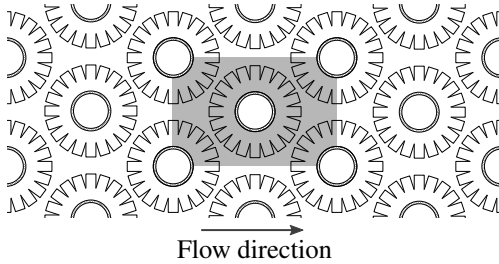


Figure 2: The numerical domain (shaded in grey) inside an infinite tube bank, with flow direction from left to right.

domain is based on the works of Maritz et al. [15] and Lindqvist & Næss [17, 18], and can be thought of as a "unit cell" within an infinite tube bank, as illustrated in Fig. 2. This implies periodicity in all directions, and reduces the computational requirements significantly, compared to domains that include several tube rows.

3.2. Governing equations

The incompressible continuity, momentum and energy equations are solved in the gas region. The continuity equation reads

$$\nabla \cdot \mathbf{u} = 0, \quad (3.1)$$

where \mathbf{u} is the velocity field. Cyclic boundary conditions in the stream wise direction necessitate the addition of a source term in the momentum equations to drive the flow, as demonstrated by Patankar & Liu [20], and takes the form,

$$\frac{\partial \mathbf{u}}{\partial t} + \mathbf{u} \cdot \nabla \mathbf{u} = \mathbf{S} - \frac{1}{\rho} \nabla p + \nabla \cdot \left[\nu_{\text{eff}} \left(\nabla \mathbf{u} + (\nabla \mathbf{u})^T \right) \right], \quad (3.2)$$

where p is the pressure field, ρ is the density and ν_{eff} is the effective kinematic viscosity. The source term \mathbf{S} acts as an imposed pressure gradient to drive the flow through the domain. The energy equation is formulated using the specific enthalpy, viz.

$$\frac{\partial(\rho h + e_K)}{\partial t} + \nabla \cdot (\mathbf{u}(\rho h + e_K)) - \frac{Dp}{Dt} = -\nabla \cdot \mathbf{q} \quad (3.3)$$

where the heat flux is given by Fourier's law $\mathbf{q} = \rho \alpha_{\text{eff}} \nabla h$, where $\alpha_{\text{eff}} = \kappa_{\text{eff}} / (\rho c_p)$ is the effective thermal diffusivity and $e_K = \frac{1}{2} \rho |\mathbf{u}|^2$ is the specific kinetic energy. The energy equation is also solved in the solid region, being a special case of Eq. (3.3) by setting $\mathbf{u} = \mathbf{0}$, $Dp/Dt = 0$ and use ρ , c_p and κ for the solid.

3.3. Choice of turbulence model

The model of choice in the present study is the *Spalart-Allmaras* turbulence model [21], which has shown good performance for flow over finned tube bundles [17, 22]. Being a one-equation model, where a transport equation for the modified turbulent viscosity $\tilde{\nu}$ is solved, it is computationally advantageous to the more common two-equation models.

3.4. Thermal properties

The unit cell allows for the assumption of constant thermal properties, as the temperature differences will be moderate since only one tube row is considered. As a consequence, the incompressibility assumption is used in the governing equations.

Both the fluid and solid regions are modelled using constant thermal properties, given in Tab. 2. The fluid is modelled as dry air at atmospheric pressure and 300 K, which matches the experimental conditions closely. The fins are modelled as carbon steel and aluminium 6060 for the Næss (N1 and N2) and Holfeld (H8) cases, respectively.

3.5. Grid generation

One of the main tasks has been to develop a parameterized grid generation procedure able to produce quality grids from a given set of geometry parameters, e.g. the result from an HRSG optimization. Lindqvist [17] had a similar approach, but limited the tube layout angle to $\beta = 30^\circ$. The present grid generation procedure is not limited to one layout angle, but rather lets β be a free variable. Fig. 3 shows one of the grids used (N2), with $\beta = 45^\circ$.

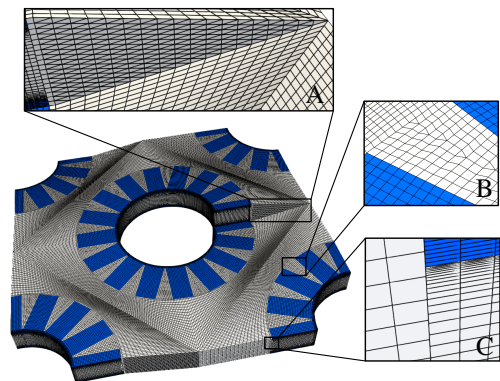


Figure 3: The numerical grid for geometry N2, showing the gas (■) and fin (■) regions.

The grid is dominated by hexagonal cells, though this is not achieved in the serrated regions, where prismatic wedge cells also are included, shown in box B in Fig.

Table 2: Thermal properties for dry air, carbon steel and aluminium A6060 at atmospheric pressure and 300 K [23, 24].

Property	Dry air	Carbon Steel	Aluminium	Unit
Thermal conductivity λ	0.0263	48.5	210	W/(m·K)
Specific heat capacity c_p	1007	434	898	J/(kg·K)
Density ρ	1.1614	7854	2700	kg/m ³
Viscosity ν	$15.89 \cdot 10^{-6}$	-	-	kg/(m·s)

3. Hexagonal cells are desired in order to maximize the accuracy of solution, and consideration was also given to skewness and cell growth to ensure a smooth grid.

The boundary layer is resolved in the inter-fin regions and on the tube surface, as shown in box C in Fig. 3. Ensuring a first cell height of $y^+ < 1$ yields a resolved turbulent boundary layer in these regions. The boundary layer cells are set to a growth rate of 20 % with a smooth transition to the inter-fin region. On the fins sides and ends however, the boundary layer was not resolved, and the turbulent boundary layer is modelled using Spalding's unified wall function [25]. At the interface between the bulk grid and the inter-fin grid, polyhedral cells are used to make the two grid regions conform. This can result in skewed faces, but is always kept within the grid criterion set in OpenFOAM. Polyhedral cells are also used in the cut-plane directly downstream of the tube, shown in box A in Fig. 3. This is a consequence of the helix angle of the fins, and results in wedge-shaped faces in order to make the periodic boundaries conform, shown in box A in Fig 3.

3.6. Boundary conditions

The fin and tube surfaces are prescribed the no-slip and no penetration boundary conditions for velocity, i.e. $\mathbf{u}_w = \mathbf{0}$ (where the subscript w denotes the quantity evaluated at the wall) and zero gradient for pressure, $\partial p_w / \partial n = 0$.

For the modified turbulent viscosity $\tilde{\nu}$, the wall boundary conditions should also be zero, i.e. $\tilde{\nu}_{t,w} = 0$. This is done on all walls except for the fin sides, where the boundary layer is not resolved. Here, wall functions are used for the turbulent viscosity directly to impose the theoretical turbulent boundary layer profiles onto the flow field. This does not yield as accurate results as the fully resolved boundary layers do, but as these constitute only a minor part of the total wall area, the use of wall functions here is deemed acceptable.

The temperature at the tube surface and fin bases is set to a uniformly fixed temperature $T_w = 300$ K at the tube walls and the base of the fins. At the interface between the gas and fins, the boundary conditions are set to a conserved heat flux through the interface as well as identical temperature for both regions, viz.

$$T_{w,\text{fluid}} = T_{w,\text{solid}}, \quad \mathbf{q}_{w,\text{fluid}} = -\mathbf{q}_{w,\text{solid}}. \quad (3.4)$$

All but the wall surfaces are periodic boundaries, and for velocity and pressure stream wise periodicity is implemented in Eq. (3.2), and the modified turbulent viscosity $\tilde{\nu}$ is also assumed to be fully periodic. The temperature is also cyclic between inlet and outlet, but an offset is prescribed to account for the temperature drop over the tubes. The offset is defined such that the left cyclic boundary (the inlet) $T_{\text{inlet}}(\mathbf{x})$ always is kept at a constant average temperature $T_{\text{in}} = 320$ K while at the same time maintaining the constant wall temperature $T_w = 300$ K,

$$T_{\text{inlet}}(\mathbf{x}) = T_w + \left(\frac{T_{\text{in}} - T_w}{T_{\text{out}} - T_w} \right) (T_{\text{outlet}}(\mathbf{x}) - T_w), \quad (3.5)$$

where $T_{\text{outlet}}(\mathbf{x})$ is the temperature field at the right cyclic boundary (the outlet) and T_{out} is the average temperature at the outlet.

For the steady-state simulations, the stream wise velocity boundary conditions are implemented by mapping the velocity and pressure fields between inlet and outlet, as were proposed by Lindqvist & Næss [17]. This improves the stability of the simulation and makes it easier to arrive at the steady-state solution. The inlet boundary is initially prescribed a uniform profile with a fixed mass flux and a zero gradient pressure, whereas the outlet is zero-gradient velocity and fixed pressure boundary condition. The velocity field is then mapped from outlet to inlet after every 1000 iterations, while the pressure field is mapped from inlet to outlet and scaled to ensure a constant pressure at the outlet boundary. This mapping is repeated until the simulation converges, which is assessed by total heat transfer and pressure drop over the central tube.

For the transient simulations, the inlet and outlet boundaries were cyclic for both the velocity and pressure fields, which is achieved by a momentum source term \mathbf{S} in Eq. (3.2), acting as an imposed pressure gradient. The pressure gradient was fixed for each simulation and corresponded to a Reynolds number. To estimate the pressure gradient to achieve a desired Reynolds number, the Weierman correlation [26] was used. The transient simulations are carried out for 20 domain flow-through cycles to ensure fully developed flow conditions.

3.7. Discretization and solution algorithm

All convective terms were discretized with the linear upwind scheme, and a linear blend between Euler (0.3) and the Crank-Nicolson (0.7) scheme was used for transient terms, giving 2nd order accuracy in space and 1st-2nd order in time.

The discretized equations were first solved with a steady state solver using the SIMPLE algorithm. The PISO algorithm was used to perform the transient simulations, with adaptive time stepping ensuring that $Co < 0.5$ for all cells in the grid. To accelerate the transient simulations, the initial conditions were obtained by carrying out steady simulations for 1000 iterations.

3.8. Data reduction

To allow for direct comparison with experimental results, non-dimensional parameters are calculated by integrating the raw numerical data and normalizing with appropriate characteristic scales.

3.8.1. Reynolds number

The Reynolds number that characterizes the flow field is defined as

$$Re = \frac{d_o u_{F_{\text{min}}}}{\nu}, \quad (3.6)$$

where $u_{F_{\text{min}}}$ is the average velocity in the minimum free flow area. In the steady-state simulations, $u_{F_{\text{min}}}$ is fixed by the inlet velocity, whereas for the transient simulations it is obtained by sampling the mean velocity at the inlet and time-averaging.

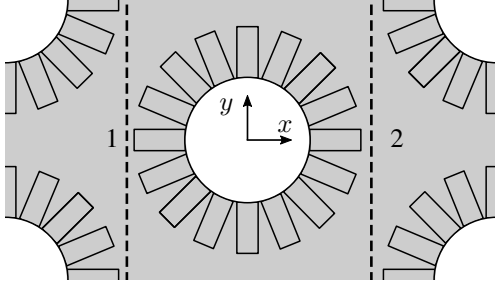


Figure 4: Sampling planes for temperature and pressure.

3.8.2. Euler number

The pressure drop is normalized by the dynamic pressure to form the Euler number,

$$Eu = \frac{\Delta p}{\frac{1}{2} \rho u_{F_{min}}^2} \quad (3.7)$$

where Δp is the pressure drop across one tube row. For the steady-state simulations, Δp is obtained by sampling the pressure in front of and behind the central tube (at $x = \pm P_l/2$). For the transient simulations, Δp is obtained by multiplying the momentum source from Eq. (3.2) with the longitudinal tube pitch P_l .

3.8.3. Nusselt number

The outside heat transfer coefficient α_o is defined as,

$$\alpha_o = \frac{\dot{Q}_{tot}}{[\eta_f A_f + A_t] \Delta T}, \quad (3.8)$$

where \dot{Q}_{tot} is the total heat transferred to both the fin and tube surface, η_f is the fin efficiency and A_f and A_t is the surface area of the fin and bare tube surfaces, respectively. ΔT is the average temperature difference that drives the heat transfer between the gas and the surface of the finned tube. For the cyclic domain with only one tube row, a local arithmetic average temperature is used to approximate the mean temperature difference,

$$\Delta T = \frac{1}{2} [(T_{b,1} - T_w) + (T_{b,2} - T_w)], \quad (3.9)$$

where $T_{b,1}$ and $T_{b,2}$ are the average bulk fluid temperatures on sampling planes located at $x = \pm P_l/2$, respectively (see Fig. 4).

In experimental studies, the fin efficiency is usually estimated using theoretical and corrected predictions, and therefore the calculated heat transfer coefficient will depend on the chosen fin efficiency calculation. On the other hand, CFD results provides a full description of the temperature field, which allows for direct computation of the actual fin efficiency. However, to compare with the experiments by Næss [19] and Holfeld [5] on a consistent basis, the corrected and theoretical approaches will be used here.

$$\eta_{th} = \frac{\tanh[m(l_e + t_f/2)]}{m(l_e + t_f/2)}, \quad (3.10)$$

where $m = \sqrt{\frac{2\alpha_o(t_f + w_f)}{k_f \cdot t_f \cdot w_f}}$.

Due to the non-uniform distribution of the heat transfer coefficient, Weierman [26] proposed the following correction

$$\eta_f = \eta_{th} \cdot (0.9 + 0.1 \cdot \eta_{th}), \quad (3.11)$$

for serrated fin tube bundles. This correction is used by Næss [19], i.e. for cases N1 and N2. For solid fins, the theoretical fin efficiency is given as,

$$\eta_{th} = C \frac{I_1(mr_f) K_1(mr_o) - I_1(mr_o) K_1(mr_f)}{I_0(mr_o) K_1(mr_f) + I_1(mr_f) K_0(mr_o)}, \quad (3.12)$$

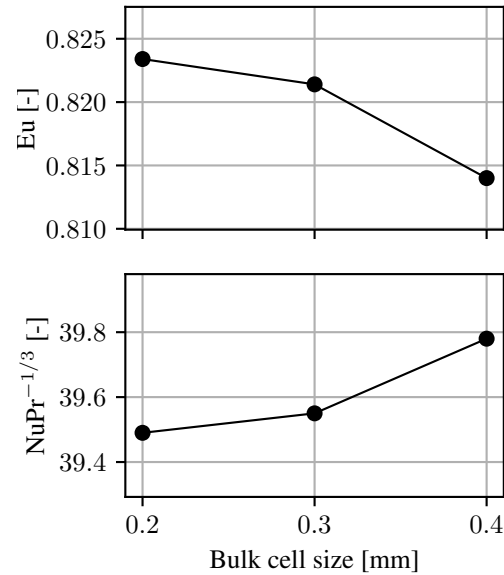
where $C = \frac{2r_o}{m(r_f^2 - r_o^2)}$ and I_n and K_n are the modified Bessel functions of first and second kind, respectively. $r_o = d_o/2$ is the tube outside radius and $r_f = r_o + h_f$ is the fin radius.

The heat transfer coefficient α_o is then normalized with d_o and κ to yield the Nusselt number, defined as

$$Nu = \frac{d_o \alpha_o}{\kappa}. \quad (3.13)$$

3.9. Grid Refinement Study

A grid refinement study was performed using the steady-state solution method on geometry H8 at $Re = 5000$. Three different grid resolutions were investigated, where the bulk mesh was refined, and the boundary layer mesh was kept at a constant y^+ and cell growth ratio. Both Eu and $NuPr^{-1/3}$ were used as integral parameters. The results from the grid refinement study can be seen in Fig. 5.

Figure 5: Results from the grid refinement study, where Eu and $NuPr^{-1/3}$ are used as integral parameters.

4. Results and Discussions

The numerical results from case H8 are shown in Fig. 6, and are compared with the experimental data from Holfeld [5] and the Weierman [26] correlation. The steady-state results are within 15% for both heat transfer and pressure drop, whereas the transient results are within 15% for pressure drop and 20% for heat transfer. All numerical results are predicting better than the Weierman correlation. Though both solution methods match the experimental results closely, it is worth noting that the transient results, which are computationally more intensive, are generally performing poorer than the steady-state simulations.

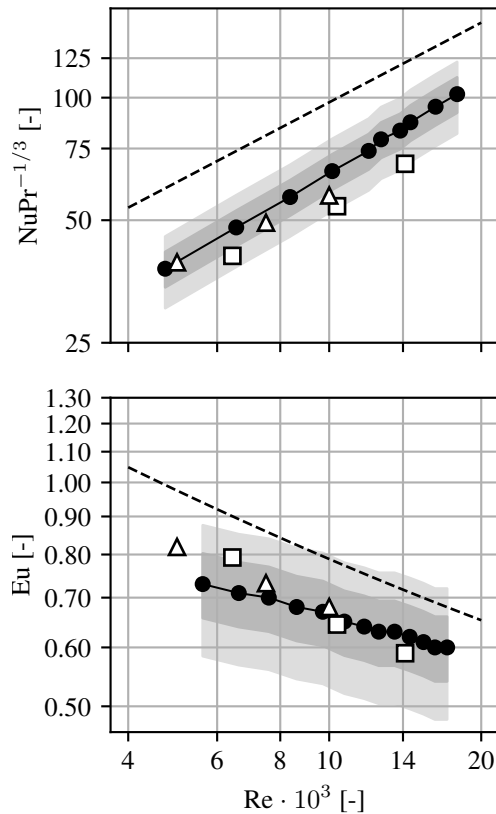


Figure 6: Results for geometry H8. Steady-state (Δ) and transient (\square) CFD results compared with the experimental results (\bullet) from Næss [19] and the Weierman [26] correlation (---). The dark and light shaded areas denote $\pm 10\%$ and $\pm 20\%$ deviation from the experimental results, respectively.

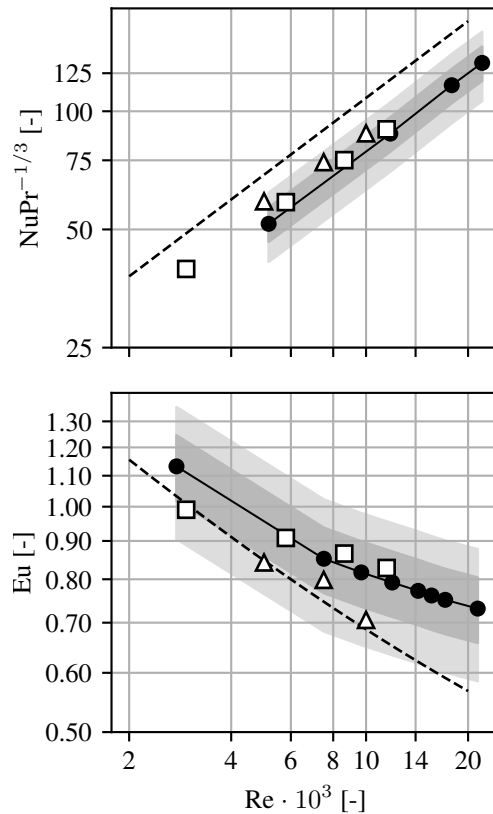


Figure 7: Results for geometry N1. Steady-state (Δ) and transient (\square) CFD results compared with the experimental results (\bullet) from Næss [19] and the Weierman [26] correlation (---). The dark and light shaded areas denote $\pm 10\%$ and $\pm 20\%$ deviation from the experimental results, respectively.

The numerical results from case N1 are shown in Fig. 7, and are compared with the experimental data from Næss [19] and the Weierman correlation. The steady-state results are within 20% for both heat transfer and pressure drop, whereas the transient results are within 10% for pressure drop and heat transfer. It is evident that the transient simulations are performing better in this case, particularly when considering the pressure drop. Eu from the steady-state simulations follows the Weierman correlation – which diverges from experiments at higher Re – closely, whereas the transient simulation matches the experimental results, but with larger deviation for the lowest Re .

The numerical results from case N2 ($\beta = 45^\circ$) are shown in Fig. 9, and are compared with the experimental data from Næss [19] and the Weierman correlation. The steady-state results did not converge, and thus only transient results are presented from this case. The convergence issues are due to the backflow at the outlet boundary. This occurs because the layout angle is so large that the wake extends beyond the outlet, resulting in unphysical and unstable behaviour. Fig. 8 shows how the wake is being limited by the zero-backflow boundary condition at the outlet. This problem is not encountered in the transient cases, where actual cyclic boundary conditions are used, and not mapping between inlet and outlet. Cyclic boundary conditions were also tested on the steady-state cases for all geometries, but all simulations displayed unstable behaviour and no converged results were obtained. The transient heat transfer results show good agreement with experimental data, being within 10% and performing significantly better than the Weierman

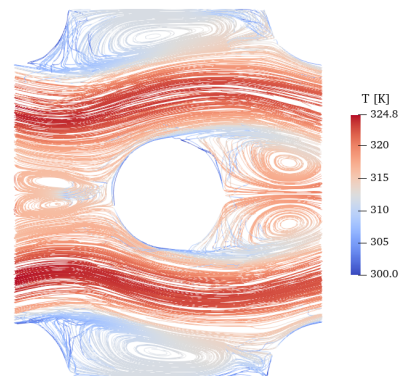


Figure 8: Streamlines coloured by temperature at $Re = 10\,000$ for geometry N2, from steady-state simulation with mapped inlet and outlet.

correlation. The pressure drop results are within 20% for all Re , but are more accurate for lower Re . The Weierman correlation displays similar accuracy. The inability of the steady-state solution method to model high layout angles is not ideal, as the transient method is computationally far more demanding and time-consuming than the steady-state approach. As the compact tube layout angle is the most used, especially for compact HRSGs, this will not be an issue in most practical cases. However, in the general case, where optimized designs may have a higher layout angle, the numerical model will not provide results as rapidly as for compact layouts.

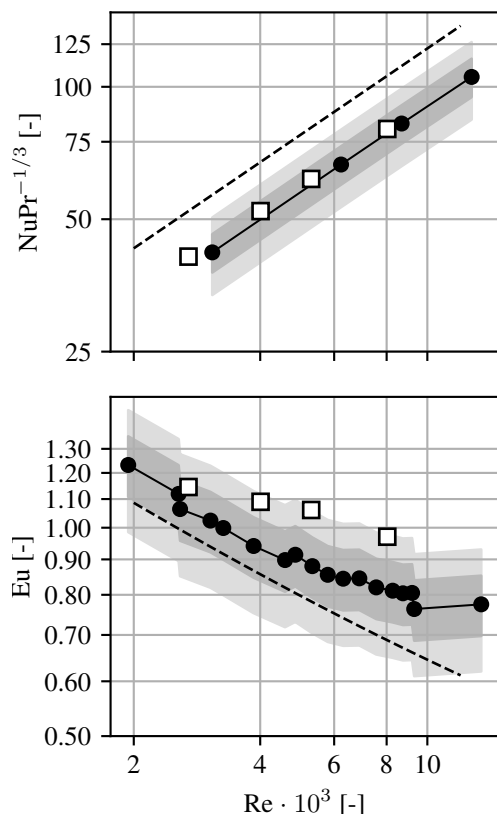


Figure 9: Results for geometry N2. Transient (\square) CFD results compared with the experimental results (\bullet) from Næss [19] and the Weierman [26] correlation (---). The dark and light shaded areas denote $\pm 10\%$ and $\pm 20\%$ deviation from the experimental results, respectively.

5. Conclusion and further work

In this study, a numerical model has been used to predict pressure drop and heat transfer in fin tube banks. A parameterized grid generation procedure was developed and used to generate grids for three different fin-tube geometries, representable for compact Heat Recovery Steam Generators. A combination of both solid and serrated fins were considered, where the serrated geometry were investigated at two different layout angles. Steady-state and transient CFD-simulations were performed on all geometries, and available experimental data was used to validate the numerical results in addition to comparison with an empirical correlation.

- All simulations were within $\pm 20\%$ of experimental data for both pressure drop and heat transfer, except for the non-converging steady-state simulations of the geometry with the largest tube layout angle.
- For compact layout angles ($\beta = 30^\circ$), steady-state simulations should be used, as they require less CPU-hours than the transient solution method. For larger layout angles, transient methods must be employed. Further work is needed to find the critical layout angles where
- To ensure sufficiently small time-steps for the transient simulations, a temporal convergence study should be performed in addition to spatial (grid) convergence studies for all geometries.
- Though being computationally more intensive, the transient solution method can also be used to perform

vibrational analyses of fin tube banks, in addition to predicting pressure drop and heat transfer.

Acknowledgment

This article is based on a Master's thesis from NTNU with computations performed at the IDUN [27] cluster. This work has been funded by HighEFF - Centre for an Energy Efficient and Competitive Industry for the Future, an 8 year Research Centre under the FME-scheme (Centre for Environment-friendly Energy Research, 257632/E20). The authors gratefully acknowledge the financial support from the Research Council of Norway and user partners of HighEFF.

References

- [1] "Klima- og miljørapport," tech. rep., Norsk Olje og Gass, 2021.
- [2] L. Nord and O. Bolland, "Steam bottoming cycles offshore – Challenges and possibilities," *Journal of Power Technologies*, vol. 92, pp. 201–207, Jan. 2012.
- [3] R. M. Montañés, G. Skaugen, B. Hagen, and D. Rohde, "Compact Steam Bottoming Cycles: Minimum Weight Design Optimization and Transient Response of Once-Through Steam Generators," *Frontiers in Energy Research*, vol. 9, p. 687248, June 2021.
- [4] M. J. Mazzetti, B. A. L. Hagen, G. Skaugen, K. Lindqvist, S. Lundberg, and O. A. Kristensen, "Achieving 50% weight reduction of offshore steam bottoming cycles," *Energy*, vol. 230, p. 120634, Sept. 2021.
- [5] A. Holfeld, *Experimental investigation of heat transfer and pressure drop in compact waste heat recovery units*. Doctoral theses, Norwegian University of Science and Technology, Trondheim, June 2016.
- [6] J.-Y. Jang, J.-T. Lai, and L.-C. Liu, "The thermal-hydraulic characteristics of staggered circular finned-tube heat exchangers under dry and dehumidifying conditions," *International Journal of Heat and Mass Transfer*, vol. 41, pp. 3321–3337, Nov. 1998.
- [7] M. S. Mon, *Numerical Investigation of Air-Side Heat Transfer and Pressure Drop in Circular Finned-Tube Heat Exchangers*. PhD thesis, Technischen Universität Bergakademie Freiberg, Freiberg, Germany, Feb. 2003.
- [8] M. S. Mon and U. Gross, "Numerical study of fin-spacing effects in annular-finned tube heat exchangers," *International Journal of Heat and Mass Transfer*, vol. 47, pp. 1953–1964, Apr. 2004.
- [9] M. Torresi, A. Saponaro, S. Camporeale, and B. Fortunato, "CFD Analysis of the Flow Through Tube Banks of HRSG," (Berlin, Germany), pp. 1–11, 2008.
- [10] S. R. McIlwain, "A Comparison of Heat Transfer Around a Single Serrated Finned Tube and a Plain Finned Tube," *International Journal of Research and Reviews in Applied Sciences*, vol. 2, pp. 88–94, Feb. 2010.
- [11] S. R. McIlwain, "A CFD Comparison of Heat Transfer and Pressure Drop Across Inline Arrangement Serrated Finned Tube Heat Exchangers With an Increasing Number of Rows," *International Journal of Research and Reviews in Applied Sciences*, vol. 4, pp. 162–169, Aug. 2010.
- [12] A. Lemouedda, A. Schmid, E. Franz, M. Breuer, and A. Delgado, "Numerical investigations for the optimization of serrated finned-tube heat exchangers," *Applied Thermal Engineering*, vol. 31, pp. 1393–1401, June 2011.
- [13] R. Hofmann and H. Walter, "Experimental and Numerical Investigation of the Gas Side Heat Transfer and Pressure Drop of Finned Tubes—Part II: Numerical Analysis," *Journal of Thermal Science and Engineering Applications*, vol. 4, p. 041008, Dec. 2012.
- [14] C. T. Ó Cléirigh and W. Smith, "Can CFD accurately predict the heat-transfer and pressure-drop performance of finned-tube bundles?," Dec. 2014. Publisher: Elsevier.

- [15] E. Martinez, W. Vicente, M. Salinas-Vazquez, I. Carvajal, and M. Alvarez, "Numerical simulation of turbulent air flow on a single isolated finned tube module with periodic boundary conditions," *International Journal of Thermal Sciences*, vol. 92, pp. 58–71, June 2015.
- [16] E. Martinez-Espinosa, W. Vicente, M. Salinas-Vazquez, and I. Carvajal-Mariscal, "Numerical Analysis of Turbulent Flow in a Small Helically Segmented Finned Tube Bank," *Heat Transfer Engineering*, vol. 38, pp. 47–62, Jan. 2017. Publisher: Taylor & Francis _eprint: <https://doi.org/10.1080/01457632.2016.1156396>.
- [17] K. Lindqvist and E. Naess, "A validated CFD model of plain and serrated fin-tube bundles," *Applied Thermal Engineering*, vol. 143, pp. 72–79, Oct. 2018.
- [18] K. Lindqvist and E. Naess, "NUMERICAL MODELING OF VORTEX SHEDDING IN HELICALLY WOUND FINNED TUBE BUNDLES IN CROSS FLOW," in *International Heat Transfer Conference 16*, (Beijing, China), pp. 1843–1850, Begellhouse, 2018.
- [19] E. Naess, "Experimental investigation of heat transfer and pressure drop in serrated-fin tube bundles with staggered tube layouts," *Applied Thermal Engineering*, vol. 30, pp. 1531–1537, Sept. 2010.
- [20] S. V. Patankar, C. H. Liu, and E. M. Sparrow, "Fully Developed Flow and Heat Transfer in Ducts Having Streamwise-Periodic Variations of Cross-Sectional Area," *Journal of Heat Transfer*, vol. 99, pp. 180–186, May 1977.
- [21] P. Spalart and S. Allmaras, "A one-equation turbulence model for aerodynamic flows," in *30th Aerospace Sciences Meeting and Exhibit*, (Reno, NV, U.S.A.), American Institute of Aeronautics and Astronautics, Jan. 1992.
- [22] H. Nematy and M. Moghimi, "Numerical Study of Flow Over Annular-Finned Tube Heat Exchangers by Different Turbulent Models," vol. 6, p. 13, 2014.
- [23] F. Incropera, D. DeWitt, T. Bergman, and A. Lavine, *Principles of Heat and Mass Transfer*. John Wiley & Sons Singapore Pte. Limited, 2013.
- [24] "Information on Aluminium 6060 - Thyssenkrupp Materials (UK)."
- [25] D. B. Spalding, "A Single Formula for the "Law of the Wall"," *Journal of Applied Mechanics*, vol. 28, pp. 455–458, Sept. 1961.
- [26] C. Weierman, "Correlations Ease the Selection of Finned Tubes," *Oil and Gas Journal*, pp. 94–100, Sept. 1976.
- [27] M. Sjalander, M. Jahre, G. Tufte, and N. Reissmann, "EPIC: An Energy-Efficient, High-Performance GPGPU Computing Research Infrastructure," *arXiv:1912.05848 [cs]*, Sept. 2021. arXiv: 1912.05848.